Valdés-Tabernero, M.A., et al. Effect of ultrafast heating on the properties of the microconstituents in a low-carbon steel, In: *Metallurgical and Materials Transactions A* 49 (2018), Pp. 3145-3150.

DOI: https://doi.org/10.1007/s11661-018-4658-4

Communication

Effect of Ultrafast Heating on the Properties of the Microconstituents in a Low-Carbon Steel

M.A. VALDES-TABERNERO, F. VERCRUYSSE, I. SABIROV, R.H. PETROV, M.A. MONCLUS, and J.M. MOLINA-ALDAREGUIA

The effect of ultrafast heating on the microstructure and properties of a low-carbon steel is studied at the microscale. Ultrafast heating results in the formation of a complex multiphase microstructure containing mainly martensite and retained austenite grains embedded into a ferritic matrix. The ferritic matrix exhibits a microstructure consisting of recovered and recrystallized grains. The recrystallized grains are softer and display pop-in events during nanoindentation, while the harder recovered grains show uniform deformation behavior.

The importance of the heating rate in steel processing is explained by the great variety of microstructures, and thus, of properties that can be derived therefrom. Processing of steels *via* ultrafast heating with heating rates in the range of 100 to 1200 °C/s followed by a very short annealing time (0.2 to 10 seconds) and rapid quenching has recently attracted the attention of the steel research community.[1,2] This interest is due to several advantages offered by ultrafast heating: the dramatic reduction in the total duration of thermal treatments (from hours to seconds), the significant decrease in energy consumption, the positive environmental effect due to a lower carbon emission during steel manufacturing, and the possibility to produce leaner alloys.[3] A body of research on the effect of ultrafast heating on the microstructure and properties of low-carbon steels already exists in the current literature. It has been demonstrated that ultrafast heating shifts the recrystallization temperature to higher values than that at conventional heating rates[4,5] and results in grain refinement,[6] which strongly depends on carbon content, degree of cold reduction prior to ultrafast heating, and initial microstructure.[4] In turn, the finer grain size results in improved mechanical strength and ductility. For example, the yield strength of a low-carbon steel was reported to increase considerably after ultrafast heating ($\Delta\sigma_y \sim 200$ MPa) with respect to a conventional heat treatment.[6] The effect of heating rate on phase composition and volume fraction of individual microconstituents was also studied.[5,7,8] Ultrafast heating of a low-carbon steel to intercritical peak temperature led to a complex microstructure of the ferritic matrix, which consisted of recrystallized and recovered grains.[5,9] Therefore, the local mechanical behavior of the ferritic matrix might dramatically vary depending on the local dislocation density. The main objective of the current study was to study the effect of ultrafast heating rate on the microstructure and mechanical behavior of individual microconstituents in a low-carbon steel laying special emphasis on the microstructure and local properties of the ferritic matrix.

A low-carbon steel Fe-0.19C-1.61Mn-1.06Al-0.50Si (in wt pct) was chosen for this study. The material was supplied in the form of 1 mm cold-rolled (50 pct reduction ratio) strips with a ferritic–pearlitic microstructure. Flat specimens with a length of 90 mm and a width of 10 mm were machined along the rolling direction. Heat treatments were carried out in a Gleeble 3800 thermomechanical simulator. A *K*-type thermocouple was spot welded to the midsection of each specimen, and the temperature during heat treatment was controlled with an accuracy of ± 1 °C. Two types of heat treatment were performed. First, ultrafast heat treatment with a heating rate of 800 °C/s to the intercritical temperature of 860 °C was followed by a very short soaking for 0.2 seconds and rapid air cooling to room temperature at ~ 160 °C/s. In the second treatment, a conventional heating rate of 10 °C/s was applied, and other heat-treatment parameters were kept the same as in the first treatment. Such a short soaking time (0.2 seconds) allows to eliminate the effect of annealing time on the microstructure and, therefore, to focus this study entirely on the effect of heating rate. The minimum length of the homogeneously heat-treated zone in each specimen was at least 10 mm, which was proven by hardness measurements and microstructural characterization along the sample length.

M.A. VALDES TABERNERO, I. SABIROV, M.A. MONCLUS, and J.M. MOLINA ALDAREGUIA are with the IMDEA Materials Institute, Calle Eric Kandel 2, 28906 Getafe, Madrid, Spain. Contact e mail: miguelangel.valdes@imdea.org F. VERCRUYSSE is with the Department of Electrical Energy, Metals, Mechanical Constructions & Systems, Ghent University, Technologiepark 903, 9052 Ghent, Belgium. R.H. PETROV is with the Department of Electrical Energy, Metals, Mechanical Constructions & Systems, Ghent University and also with Delft University of Technology, Department of Materials Science and Engineering, Mekelweg 2, 2628CD Delft, The Netherlands.

Manuscript submitted February 19, 2018.

The microstructure was characterized on the RD–ND plane. Specimens for scanning electron microscopy (SEM) studies were ground and polished to a mirror-like surface applying standard metallographic techniques with final polishing using OP-U (colloidal silica). The polished specimens were immersed for 10 seconds into a 3 pct Nital solution for chemical etching. Examination of the microstructure was performed using a SEM EVO MA15 operating at an accelerating voltage of 20 kV. Specimens for EBSD analysis were prepared following the same procedures as for SEM. Orientation imaging microscopy studies were performed using a FEI Helios™ NanoLab 600i, equipped with a NordlysNano detector controlled by the AZtec Oxford Instruments Nanoanalysis (version 2.4) software. The data were acquired at an accelerating voltage of 18 kV, a working distance of 8 mm, a tilt angle of 70 deg, and a step size of 65 nm in square scan grit. The orientation data were postprocessed using HKL Post-processing Oxford Instruments Nanotechnology (version 5.1©) software and TSL Data analysis version 7.3 software. Grain boundaries having a misorientation ≥ 15 deg were defined as high-angle grain boundaries (HAGBs), whereas low-angle grain boundaries (LAGBs) had a misorientation < 15 deg. The recrystallized, recovered (unrecrystallized) and transformed fractions were separated by a two-step partitioning procedure described earlier in Reference 9. The procedure is based on separating the grains with high and low grain average image qualities in the first step, which allows to distinguish between transformed (martensite) and untransformed (ferrite) fractions. In the second step, the grain average misorientation criterion is used to identify recrystallized and recovered ferritic grains. The

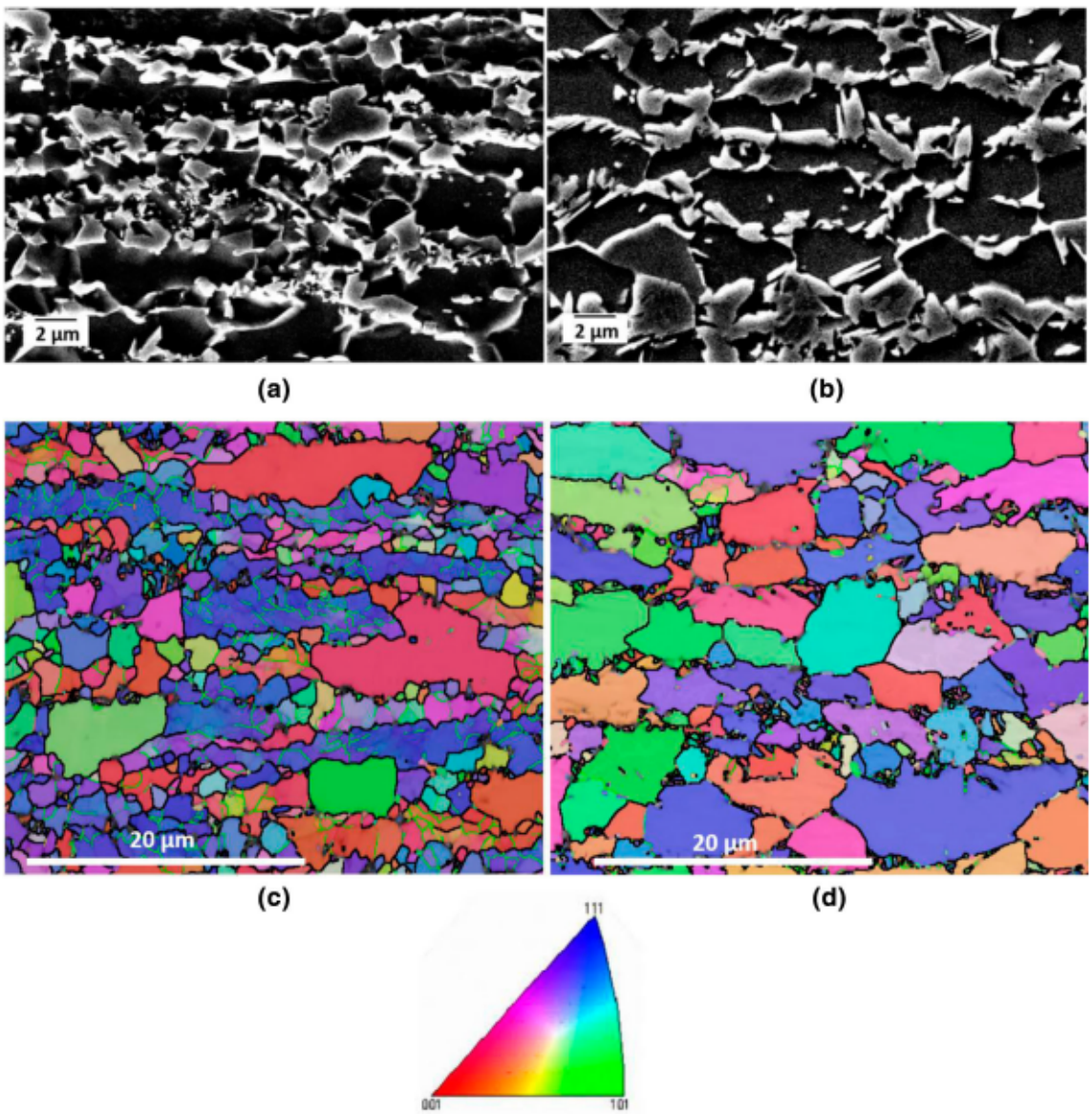

Fig. 1 SEM images of the ultrafast (*a*) and conventional (*b*) heat treated steels; ND IPF maps of the ultrafast (*c*) and conventional (*d*) heat treated steels with HAGBs (black lines) and LAGBs (green lines) (Color figure online).

density of geometrically necessary dislocations (GNDs) was calculated from the local misorientations following the procedure described in Reference 10.

Nanoindentation tests were performed on a Hysitron TI950 Triboindenter using a Berkovich tip on square areas having a size of $10 \times 10\ \mu m^2$, which were *a priori* analyzed by EBSD. At least five areas were tested for each material's condition. In order to target specific phases/grains, these square areas were scanned, prior to nanoindentation, using the scanning probe microscopy (SPM) mode of the instrument. Nanoindentation tests were carried out in displacement control mode at a constant strain rate ($\dot{\varepsilon} = \dot{h}/h$) of 0.07 s^{-1}, where h is the penetration depth and $\dot{h}$ the penetration rate of the indenter. At least 50 indents were performed on ferrite, and at least 20 indents were performed on martensite at an imposed maximum indentation depth of 150 nm. The nanohardness was determined from the analysis of the load–displacement curves using the Oliver and Pharr method.[11]

Figures 1(a) and (b) show SEM images of the microstructure of the ultrafast and conventional heat-treated steels. Both heat treatments resulted in the formation of a complex microstructure with a ferritic matrix (dark areas), quenched martensite (light gray areas) mainly distributed along bands, and a low fraction of retained austenite. Table I lists the outcomes of the quantitative analysis of the volume fractions of the individual microconstituents determined by EBSD. With the increasing heating rate, the volume fractions of the martensite and the retained austenite decrease by a factor of 2. This can be related to the shift of the Ac_1 and Ac_3 temperatures to higher values with the increasing heating rate to the ultrafast range.[5] It was also very recently reported that carbon diffusion controlled austenite formation and growth during conventional heat treatment can be replaced by the so-called massive mechanism of austenite growth upon ultrafast heat treatment.[7] However, this change of mechanism occurs at temperatures above Ac_3, whereas in our processing route, the peak temperature was in the intercritical range. Therefore, the influence of this change of austenite growth mechanism on the austenite fraction at the peak temperature (which, in turn, determines the martensite fraction after quenching) can be ruled out in our case. The fraction of recrystallized ferritic grains decreases from 69 to 34 pct with the increasing heating rate [Table I; Figures 1(c), (d) and 2]. It is seen that most of the ferritic grains in the conventional heat-treated steel are recrystallized and free of LAGBs [Figure 1(d)], while the formation of a substructure due to recovery during ultrafast heat treatment is observed in the majority of ferritic grains [Figure 1(c)]. The recrystallized grains in the ultrafast heat-treated material are finer compared to those in the conventionally treated steel (Table I). The GND maps generated for recrystallized [Figures 2(a) and (c)] and nonrecrystallized (*i.e.*, recovered) grains [Figures 2(b) and (d)] show dramatic differences in the density of GNDs in the recrystallized ($\sim 10^{13}\ m^{-2}$) and recovered (up to $\sim 5 \times 10^{14}\ m^{-2}$) grains of the ultrafast heat-treated steel, while the density of GNDs is lower in the conventionally heat-treated steel ($\sim 10^{13}$ *vs* $\sim 10^{14}\ m^{-2}$). Such effect of heating rate was earlier related to the shift of the onset of recrystallization to higher temperatures[4,5] with ultrafast heating. A longer time at elevated temperatures during the conventional heat treatment results in a more pronounced recovery of nonrecrystallized ferritic grains and, thus, in a lower GND density [Figure 2(d)] compared to the ultrafast heat-treated condition [Figure 2(b)].

Figure 3(c) illustrates typical load–depth curves from the nanoindentation experiments on individual microconstituents determined *a priori* by EBSD analysis [Figure 3(a)] and verified by SPM [Figure 3(b)]. The outcomes of nanoindentation testing are summarized in Table II. Martensitic grains in both conditions showed high nanohardness values. It should be noted that the standard deviation for the ultrafast heat-treated steel (7.6 ± 2.4 GPa) was much higher than for the conventional heat-treated material (8.1 ± 1 GPa). This observation can be related to the lower fraction of austenite formed at the peak temperature during ultrafast heat treatment, as much shorter time at high temperatures shortens the diffusion distance for carbon atoms,[5] leading to deviations in the local carbon concentration between different austenitic grains, as well as in the interior of individual grains. This results in higher standard deviation of the nanohardness values in the ultrafast heat-treated martensite (Table II), as its

Table I. Volume Fractions of Individual Microconstituents and Their Grain Size in the Heat-Treated Steels

	Martensite		Ferrite				Retained Austenite
			Nonrecrystallized		Recrystallized		
Conditions	Volume Fraction (Pct)	Grain Size (μm)	Volume Fraction (Pct)	Grain Size (μm)	Volume Fraction (Pct)	Grain Size (μm)	Volume Fraction (Pct)
Conventional Heat Treated	9.2	0.32	18.6	1.36	69.3	2.51	2.9
Ultrafast Heat Treated	5.3	0.31	59.3	1.21	34.1	1.43	1.4

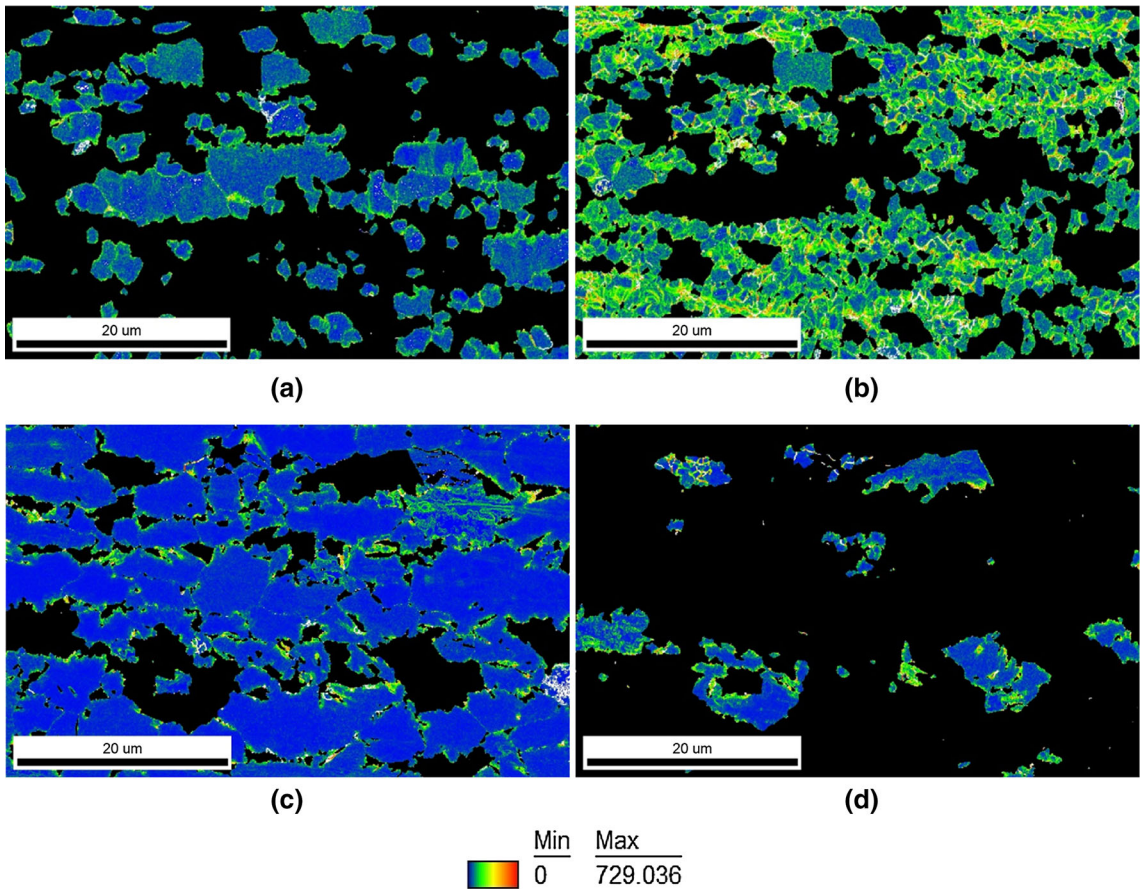

Fig. 2 EBSD maps showing density of GNDs in recrystallized grains (*a*, *c*) and nonrecrystallized grains (*b*, *d*) maps for the ultrafast (a, b) and conventional (c, d) heat treated materials (Color figure online).

hardness strongly depends on the carbon content.[12] It should be noted that all load–depth curves from measurements on different martensitic grains showed a similar continuous character [similar to indent 3 on Figure 3(c)] for both conventional and ultrafast heat-treated materials. On the other hand, ferritic grains demonstrated two different types of mechanical response during nanoindentation. Pop-ins (sudden load bursts during the loading section) on the load–depth curves were observed for the vast majority of recrystallized ferritic grains in both conventional (86 pct) and ultrafast heat-treated (96 pct) conditions [similar to indent 1 on Figure 3(c); Table II], while the curves for the remaining recrystallized grains were continuous [similar to indent 4 on Figure 3(c)]. In contrast, the fraction of the recovered ferritic grains showing pop-in events was lower for both conventional (50 pct) and ultrafast heat-treated (62 pct) conditions (Table II). Representative load–depth curves of both types for both conditions are presented in Figure 4. It is clearly seen that the critical load and depth for pop-in events can vary for different measurements. Analysis of these curves and the quantitative data provided in Table II shows that the nonrecrystallized ferritic grains exhibit higher nanohardness and lower critical loads for pop-in in both conventional and ultrafast heat-treated conditions.

The occurrence of pop-ins on nanoindentation curves has been attributed to the onset of plastic deformation due to nucleation and multiplication of dislocations in a lattice with a low density of preexisting dislocations.[13,14] Nanoindentation experiments on ferritic steels with varying dislocation densities obtained by cold rolling followed by annealing treatments clearly showed that the nanohardness and critical load for pop-in events are determined by the density of preexisting mobile dislocations.[15] It was demonstrated that the critical load for pop-in event tends to decrease with the increasing dislocation density. The pop-in effect is eliminated above certain dislocation density when the amount of preexisting mobile dislocations is sufficient to provide plastic deformation upon nanoindentation. The higher nanohardness of the recovered ferritic grains in both studied conditions is related to the higher dislocation density compared with the recrystallized grains. In turn, the nonrecrystallized ferritic grains in the conventionally heat-treated steel are softer compared with the ultrafast heat-treated material due to their lower dislocation density (Figure 2). It should be noted that different ferritic grains during cold rolling of the steel

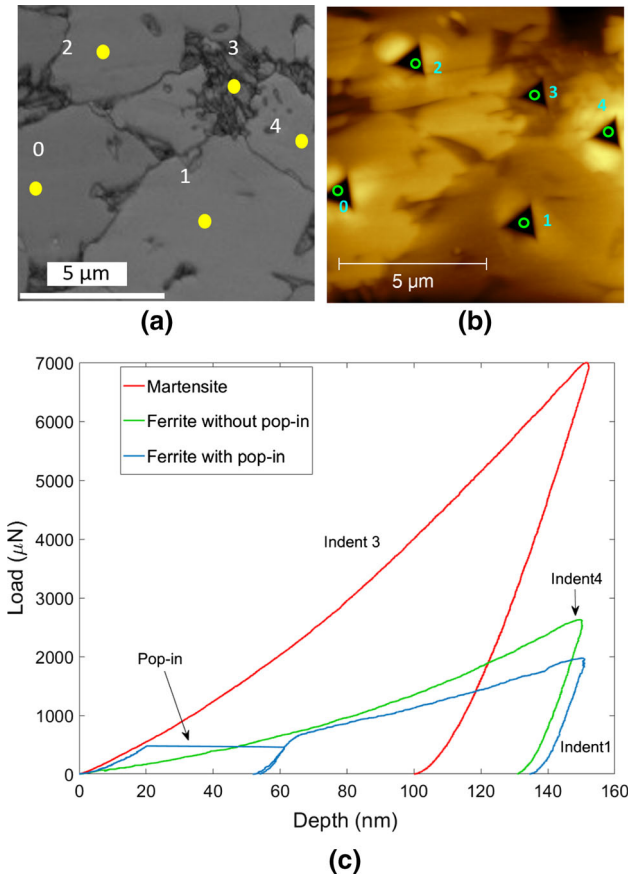

Fig. 3 Band contrast EBSD map with marked spots (grains) for nanoindentation (*a*) and SPM image of the corresponding area with indents after nanoindentation (*b*); load depth curves from nanoindentation (*c*) on spots (grains) identified in (a) (Color figure online).

Table II. Nanohardness Values for Ferrite and Martensite Grains and Percentage of Observed Pop-in Events and Their Critical Loads for Recrystallized and Nonrecrystallized Grains for the Conventional- and Ultrafast Heat-Treated Steels

Parameters/Conditions	Conventional Heat Treated	Ultrafast Heat Treated
Nanohardness of Martensite (GPa)	8.1 ± 1.0	7.6 ± 2.4
Nanohardness of Recrystallized Ferrite (GPa)	2.78 ± 0.28	2.77 ± 0.32
Nanohardness of Nonrecrystallized Ferrite (GPa)	2.99 ± 0.58	3.13 ± 0.34
Fraction of Recrystallized Ferritic Grains with Pop ins (Pct)	86	96
Critical Load for Pop in in Recrystallized Ferrite (μN)	451.1 ± 292.7	362.4 ± 218.0
Fraction of Nonrecrystallized Ferritic Grains with Pop ins (Pct)	50	62
Critical Load for Pop in in Nonrecrystallized Ferrite (μN)	255.8 ± 3.1	209.1 ± 154.6

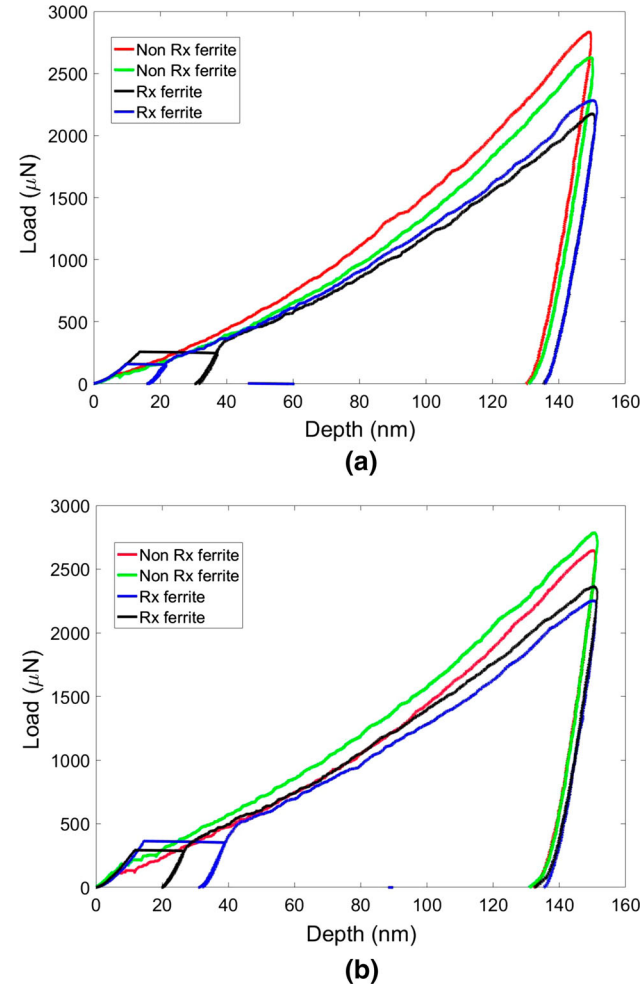

Fig. 4 Typical load depth curves from nanoindentation experiments on ferritic grains on the (*a*) ultrafast and (*b*) conventional heat treated steels. *Rx* stands for 'recrystallized,' *Non Rx* stands for 'nonrecrystallized' (Color figure online).

can accumulate different amounts of plastic strain depending on the local microstructural architecture (size of neighbor pearlitic colonies, orientation of cementite plates inside of the neighbor pearlitic colony determining its strength during rolling, *etc.*). Depending on the initial local dislocation density, the given area will undergo recrystallization or recovery during heat treatment. In the latter case, the final local dislocation density of the recovered area will be determined to a great extent by the initial local dislocation density. It should also be noted that some amount of dislocations can be introduced into recrystallized grains upon martensite formation in the neighborhood, as these ferritic grains have to accommodate the local lattice expansion due to martensitic transformation. Thus, there can be a significant variation of local dislocation density in different ferritic grains after both heat treatments resulting in such significant standard deviation of the critical load for pop-in events in both recrystallized and recovered grains (Table II).[16] The effect of crystallographic orientation of individual grains

on their mechanical response during nanoindentation can be ruled out due to the complex stress state in the plastic zone underneath the nanoindenter tip.[17]

MAVT acknowledges gratefully the financial support by IMDEA Innovation Award. IS, MAM, and JMMA would like to acknowledge the support by Madrid Region under Programme S2013/MIT-2775, DIMMAT Project. FV acknowledges the support via European Project EC-RFCS "Optimization of QP steels designed for industrial applications" (OPTIQPAP).

REFERENCES

1. T. Lolla, G. Cola, B. Narayanan, B. Alexandrov, and S.S. Babu: *Mater. Sci. Technol.*, 2011, vol. 27, pp. 863 68.
2. R.H. Petrov, J.J. Sidor, W. Kaluba, and L. Kestens: *Mater. Sci. Forum*, 2012, vols. 715 716, pp. 661 66.
3. www.flashbainite.com.
4. M. Ferry, D. Muljono, and D.P. Dunnes: *ISIJ Int.*, 2001, vol. 41, pp. 1053 64.
5. F.M. Castro Cerda, C. Goulas, I. Sabirov, S. Papaefthymiou, A. Monsalve, and R.H. Petrov: *Mater. Sci. Eng. A*, 2016, vol. 672, pp. 108 19.
6. A. Reis, L. Bracke, R. Petrov, J. Kaluba, and L. Kestens: *ISIJ Int.*, 2003, vol. 121, pp. 1260 67.
7. F.M. Castro Cerda, I. Sabirov, C. Goulas, J. Sietsma, A. Monsalve, and R.H. Petrov: *Mater. Des.*, 2017, vol. 116, pp. 448 60.
8. S. Papaefthymiou, C. Goulas, F.M. Castro Cerda, N. Geerlofs, and R. Petrov: *Steel Res. Int.*, 2017, vol. 87, pp. 999 1011.
9. F.M. Castro Cerda, L.A.I. Kestens, A. Monsalve, and R H. Petrov: *Metals*, 2016, vol. 6, pp. 288 99.
10. D.P. Field, P.B. Trivedi, and S.I. Wright: *Ultramicroscopy*, 2005, vol. 103, pp. 33 44.
11. W.C. Oliver and G.M. Pharr: *J. Mater. Res.*, 1992, vol. 7, pp. 1564 75.
12. B. Hutchinson, J. Hangstrom, O. Karlsson, D. Lindell, M. Tornberg, F. Lindberg, and M. Thuvander: *Acta Mater.*, 2011, vol. 59, pp. 5845 57.
13. A.M. Minor, S. A. Syed Asif, Z. Shan, E.A. Stach, E. Cyrankowski, T.J. Wyrobek, and O.L. Warren: *Nat. Mater.*, 2006, vol. 5, pp. 697 709.
14. T. Ohmura and K. Tsuzaki: *J. Mater. Sci.*, 2007, vol. 42, pp. 1728 39.
15. K. Sekido, T. Ohmura, T. Hara, and K. Tsuzaki: *Mater. Trans.*, 2012, vol. 53, pp. 907 1009.
16. F.J. Humphreys and M. Hatherly: *Recrystallization and Related Annealing Phenomena*, Pergamon, Oxford, 2004.
17. R. Sanchez Martin, M.T. Perez Prado, J. Segurado, and J.M. Molina Aldareguia: *Acta Mater.*, 2015, vol. 93, pp. 114 28.